Scientia Iranica B (2020) 27(5), 2478–2488

Sharif University of Technology
Scientia Iranica
Transactions B: Mechanical Engineering
http://scientiairanica.sharif.edu

Inverse design of a centrifugal pump on the meridional plane using ball-spine algorithm

H. Fallah-Ardeshir[a,*], B. Ehghaghi[a], and M. Nili-Ahmadabadi[b]

a. *Department of Mechanical Engineering, University of Tabriz, P.O. Box 51666-14766, Tabriz, Iran.*
b. *Department of Mechanical Engineering, Isfahan University of Technology, Isfahan, Iran.*

Received 23 February 2019; received in revised form 26 April 2019; accepted 2 June 2019

KEYWORDS
Inverse design;
Centrifugal pump;
Meridional plane;
Quasi-3D;
Impeller;
Viscous.

Abstract. This study developed an inverse design algorithm called Ball-Spine Algorithm (BSA) as a quasi-3D method and applied it to the meridional plane of a centrifugal pump impeller in an effort to improve its performance. In this method, numerical analyses of viscous flow field in the passage between two blades were coupled with BSA to modify the corresponding hub and shroud geometries. Here, full 3D Navier-Stokes equations were solved on a thin plane of flow instead of solving inviscid, quasi-3D flow equations on the meridional plane. To demonstrate the validity of the present work, the performance of a centrifugal pump was numerically investigated first and then, it was compared with available experimental data. After defining a target pressure distribution on the hub and shroud surfaces of the flow passage, a new impeller geometry was then obtained in accordance with the modified pressure distribution. The results indicated a good rate of convergence and desirable stability of BSA in the design of rotating flow passages with incompressible, viscous flows. Overall, the proposed design method gave rise to the following major improvements: an increase in static pressure along the streamline, a 5% increase in the pump total head, and delay in the onset of flow cavitation inside the impeller.

1. Introduction

Optimization problems related to pump design are generally challenging due primarily to the complexity of pump geometry and the corresponding flow pattern inside. The optimal design of a geometry on the meridional plane of a pump is of significance, as it directly influences the flow pattern and velocity distribution inside the impeller, hence the hydraulic performance of the pump. In addition, the velocity distribution on the shroud surface of an impeller affects the onset of flow cavitation and net positive suction head of the pump. The inverse design of the flow passage is one of the common approaches to problems of this nature. This process involves obtaining flow boundaries associated with a prescribed wall pressure or velocity profile and is generally achieved in two ways: non-iterative (coupled/direct) or iterative (non-coupled). In the former approach, a form of problem formulation can be used, in which the flow border is defined either implicitly or explicitly as a dependent variable and appears in the governing equations. In the latter method, however, flow and geometrical variables are independent of each other. These methods use an initial guess and the process is repeated until convergence is achieved. Although iterative methods are more

*. *Corresponding author. Fax: +98 4134754447*
E-mail address: fallah.hadi@tabrizu.ac.ir (H. Fallah-Ardeshir)

doi: 10.24200/sci.2019.52991.2989

general and powerful, they are often mathematically complex and computationally intensive. These methods, however, can use black-box analytics to predict flow field within the passage, facilitating the design of more complex flow passages.

Researchers have previously used different target functions to perform the design procedure [1–4]. Tiow and Zanganeh [5] and Yang and Wu [6] established the aforementioned method by applying virtual velocity to blade surfaces. Demeulenaere and Van den Braembussche [7] changed the boundary condition on the blade walls and modified the geometry by inverse design code according to target pressure distribution. Virtual velocity on blade camber line and walls has also been used previously as a design function [8-12]. Yang et al. [13] employed the formulation developed by Mileshin et al. [10] to calculate the induced virtual velocity.

Poursadegh et al. [14–16] used a ball-spine inverse design algorithm on the meridional plane of a centrifugal compressor impeller and, then, developed an original and progressive algorithm to design the blade camber line profile on the blade-to-blade planes of impeller based on blade loading improvement. Madadi et al. [17,18] employed the aforementioned design algorithm to design an axial flow compressor on the blade-to-blade surface as well as S-shaped diffusers.

Arbabi [19,20] and colleagues developed an aerodynamic inverse design method for the three-dimensional design of viscous flow in blade passages. An aerodynamic inverse shape design approach, fully consistent with viscous flow, was successfully developed for the 3D design of turbomachinery blades. Ramamurthy et al. [21] developed an inverse shape design method for steady, two-dimensional viscous internal and external flows over airfoils. In this method, a target pressure distribution was prescribed on the airfoil suction side. The approach was fully consistent with the viscous flow assumption and was incorporated into a time accurate solution of the Reynolds-averaged Navier Stokes equations. The inverse method was first validated and, then, used to redesign airfoils for internal and external flow cases, where the robustness and usefulness of the inverse method were demonstrated.

Recently, the inverse design algorithms have been extensively used to design efficient turbomachines in various applications. This clearly demonstrates the potentials of this approach in the field [22–29].

In the current work, the ball-spine inverse design algorithm is developed as a quasi-3D method and, then, applied to the meridional plane of a centrifugal pump impeller operating in an incompressible, viscous flow regime. In this method, viscous flow simulations are conducted within a thin region between two adjacent blades of an impeller, where the full 3-D Navier-Stokes equations are solved instead of their inviscid, quasi-3D counterparts. Considering the rotary nature of the frame of reference in this study, a reduced static pressure distribution [30] is used as a target parameter. The performance of the developed design method is then examined on the meridional plane of a centrifugal pump. Finally, the flow passage is designed to (a) optimize pressure gradients along the passage, (b) minimize and eliminate potential wakes, and (c) increase the discharge pressure. The designed geometry is then simulated to investigate the realization of the aforementioned targets.

2. Geometry

Impeller is the only rotating part of a pump transferring the supplied energy to the working fluid. Figure 1 presents the meridional view of a centrifugal pump. As shown earlier, the impeller blades are bounded by hub and shroud surfaces, allowing for the control of passages' cross-sectional area. The working fluid enters the impeller in the axial direction and leaves it, while its direction turns close to 90 degrees.

Table 1 summarizes the hydraulic specification of the reference geometry used for the analyses presented.

3. Ball-spine inverse design algorithm

The ball-spine method is fundamentally an iterative approach. Figure 2 demonstrates the overall procedure used for geometry modification. As shown, the hub and shroud walls are composed of virtual balls with fixed mass that can be freely moved along the specified directions called spine. Fluid flow through the passage

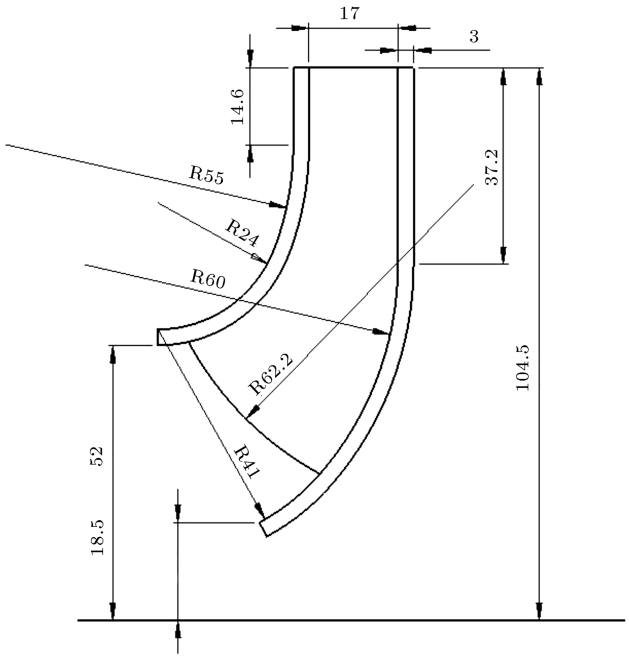

Figure 1. Meridional view of a centrifugal pump impeller.

Table 1. Features of reference impeller.

Type of pump	Radial flow pump with a shrouded impeller
Specific speed	25
Rotational speed (rpm)	1450
Design flow rate (m^3/hr)	50
Design head (m)	13
Blade number	6
Impeller eye diameter (mm)	104
Impeller exit diameter (mm)	209

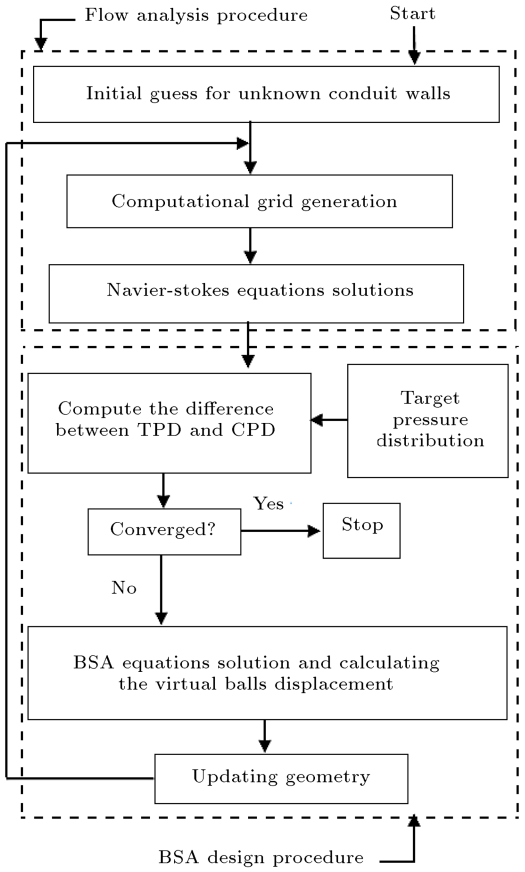

Figure 2. Implementation of the inverse design algorithm.

applies a pressure distribution to the wetted side of the boundary. If the target pressure distribution is applied to the outer side of the boundary, the flexible walls begin to deform in a way that the actual pressure inside the passage equals the target pressure. In other words, the force due to the difference between current and desired pressure profiles anywhere along the wall displaces the corresponding balls at any point along the spine. As the desired shape is achieved, the difference between two pressure profiles disappears and the balls stop moving.

Figure 3 demonstrates the free body diagram of

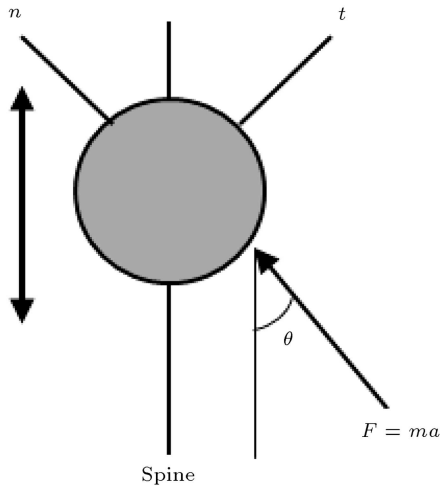

Figure 3. Free body diagram of a ball [16].

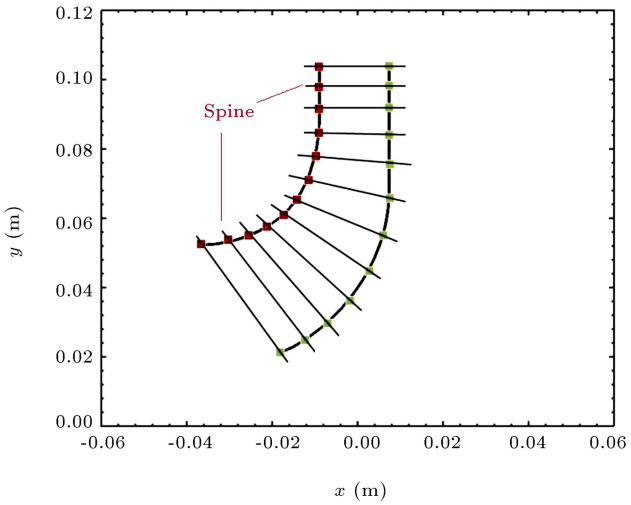

Figure 4. Schematic of spines in the meridional plane.

a virtual ball. If the balls move in the direction of applied force, adjacent balls may collide with or avoid each other. To prevent this problem, each ball should move along the spine during the entire process of deformation.

Figure 4 shows the spines for a flow passage on the meridional plane. In the current work, the spines are chosen to be perpendicular to the flow stream. In order to obtain a unique solution to the inverse design problem in hand, the axial length of the flow passage is kept constant.

According to Figure 3, the displacement of balls in each shape modification step is calculated using Eq. (1). Here, C is an adjustment parameter for the convergence rate of the BSA method. A smaller value of this parameter results in a slower convergence rate of the algorithm. Note that if the value of this adjustment parameter exceeds a certain threshold, the design algorithm will diverge [16]. Therefore, allocating an optimal value to this constant is of significant

importance to minimize the computation costs. Now, assuming that the displacement of the imaginary balls is only due to the pressure difference between the inside and outside of the boundary, we have:

$$\Delta S_i = C \times \Delta P_i, \tag{1}$$

$$F = \Delta P \cdot A \cdot \cos\theta = ma \Rightarrow a = \frac{\Delta P \cdot A \cdot \cos\theta}{m}, \tag{2}$$

$$\Delta S = \frac{1}{2}\frac{\Delta P \times A \times \cos\theta}{\rho_b \times A}(\Delta t)^2 = \frac{(\Delta t)^2}{2\rho_b} \times \Delta P \times \cos\theta, \tag{3}$$

$$C = \frac{(\Delta t)^2}{2\rho_b} \times \cos\theta. \tag{4}$$

Projecting the displacements into perpendicular horizontal and vertical displacements yields:

$$\begin{cases} \mathcal{X}_{\text{new}} = \mathcal{X}_{\text{old}} + \Delta S.\cos\alpha \\ \mathcal{Y}_{\text{new}} = \mathcal{Y}_{\text{old}} + \Delta S.\sin\alpha \end{cases} \tag{5}$$

where α denotes the angle of spine from the horizon.

In the current method, residual for the proposed iterative design process is calculated using Eq. (6). A threshold of 10^{-2} is used here to determine when convergence to the target geometry is achieved. To ensure higher accuracy, ANSYS CFX is used to solve the flow field in each iteration.

$$residual = \frac{\sum_{i=1}^{N}\left[P_i - (P_{target})_i\right]}{\sum_{i=1}^{N}\left[(P_{target})_i\right]}. \tag{6}$$

4. 3-D modeling

In this work, a 3D simulation of the centrifugal pump is conducted to examine its performance and the results are compared against the experimental data. The simulated geometry encompasses three distinct parts: impeller, volute, and outlet pipe. Figure 5 shows the overall view of the pump.

5. Mesh generation

Structured and unstructured meshes are used for mesh generation within the simulation domain. Here, an O-grid structured mesh is used in the blade near-wall region in order to examine the boundary layer better, as shown in Figure 6. In the current study, the average y^+ in the wall region is about 1.5 and its maximum value does not exceed 5.

6. Boundary conditions

Table 2 summarizes the boundary conditions used in this study. Static pressure of the reservoir is used as the inlet boundary condition. Here, an average turbulent intensity of about 1% is considered. This is justified where the turbulent intensity of flow at the inlet is minimized by existing baffles. A known mass flow rate (or the average velocity) is used at the outlet boundary. Here, the corresponding value at the Best Efficiency Point (BEP) of the pump is used. No-slip condition is enforced at the solid boundaries. The frozen rotor model is also used to calculate the average tangential velocity at the interface of stationary and rotary parts. This model utilizes a quasi-stable algorithm, which

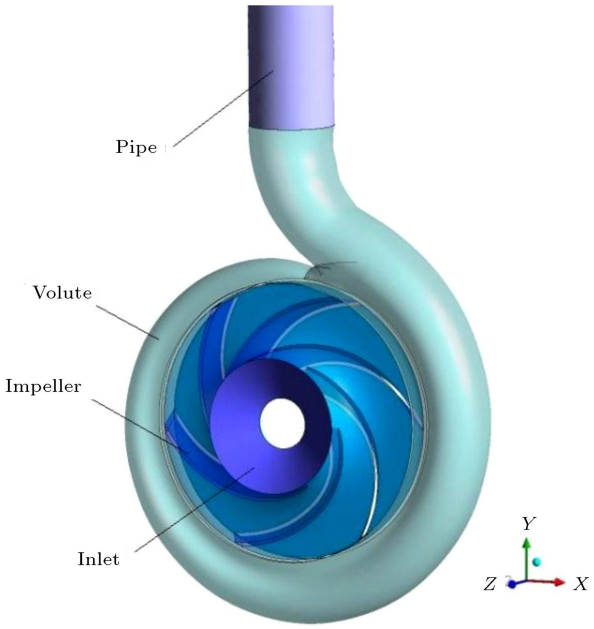

Figure 5. General view of the centrifugal pump model.

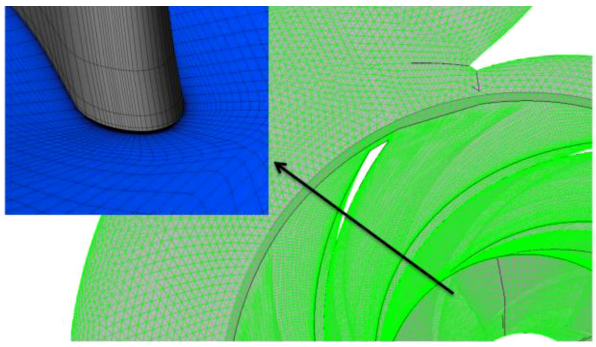

Figure 6. Mesh configuration used for flow analysis.

Table 2. Boundary condition for the numerical study of centrifugal pump.

Inlet pressure (bar)	0.15
Inlet turbulence intensity (%)	1
Outlet mass flow rate (BEP) (kg/s)	15.5
Wall roughness (μm)	100
Reference pressure (atm)	1
Physical time step (sec)	0.001

treats the flow from rotor to stator by changing the frame of reference while maintaining their relative position. The rotary terms are simulated in the moving frame of reference, but the transient effects are neglected. This leads to an effective approach to calculating the communication between the impeller and volute. Water at 25°C (with a density rate of 997 kg/m^3 and a dynamic viscosity rate of 0.0010518 Pa.s) is considered as the working fluid in this investigation. The shear stress transport model is used to simulate turbulence.

7. Mesh independency

In the current study, the outlet pressure is used as a parameter to investigate the dependency of the simulations on the used grid sizes. Table 3 summarizes the results including the impeller, volute, and the outlet pipe for the overall simulation domain. Based on these results, a domain of 2173604 elements is used to achieve a mesh-independent simulation while being still computationally affordable.

8. Result validation

In this section, the experimental data obtained from the hydraulic test of the main centrifugal pump are used to validate the simulation results. The measurements were conducted at the Turbomachinery Laboratory of the University of Tabriz. Figure 7 shows a schematic of the centrifugal pump test bed, which is fully equipped with data acquisition and analysis systems. The geometrical and design point specifications of the pump used are summarized in Table 1. Figure 8 presents a comparison between the measured and simulated pump heads in terms of flow rates. As shown, the predictions are within 5% of the measured values and, in fact, the error falls below 1% at the design point of the pump.

Table 3. Evaluation of the dependency of mesh.

Number of elements	Outlet pressure
1842482	180169
2173604	178888
3277226	178261

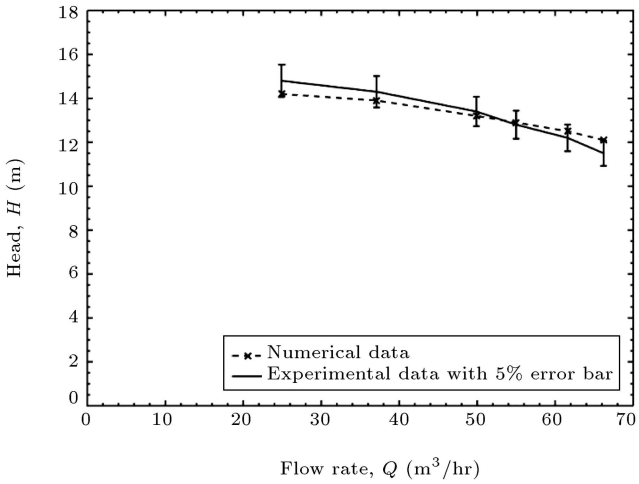

Figure 8. Comparison of numerical results and experimental results.

9. Algorithm implementation

The inverse design procedure comprises two major parts: flow solver and shape modification algorithm. Here, ANSYS CFX is used as the flow solver, and the design algorithm is implemented through a separate

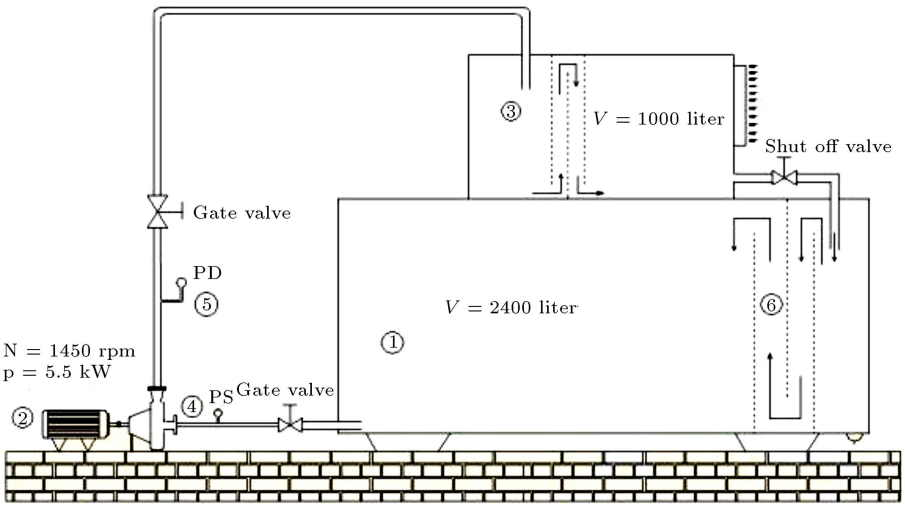

Figure 7. The schematic of the centrifugal pump test bed located at the Turbomachinery Laboratory of the University of Tabriz.

MATLAB code. The design procedure begins with a comparison between the target and initial pressure profiles on the hub and shroud boundaries. The difference between the two pressure distributions results in a change in the geometry of the flow passage at each iteration. Flow field associated with the modified geometry is then simulated using CFX, and the actual pressure profile is updated accordingly. This process is repeated until the difference between the actual and target pressure distributions falls below the predefined threshold. The current method allows for implementing different filters in order to smoothen the modified geometry and utilizing different adjustment parameters to improve the convergence rate of the algorithm.

10. Quasi-3D flow passage and boundary conditions

Considering the symmetrical geometry of the impeller and the incoming flow, the problem is simplified to a quasi-3D case in order to shorten the computation time. It is important to note that all geometrical changes occur on the meridional plane; therefore, the passage specifications on the blade-to-blade plane are not affected. The aforementioned geometry is constructed in the ICEM CFD environment such that the meridional projection rotates by about 2 degrees around the symmetry axis of the impeller, as shown in Figure 9. No-slip boundary condition is applied to the hub and shroud, while the side walls are considered to allow free flow slip. The intake of the impeller also remains unaffected during the design procedure. Note that structured grids are used in the entire computational domain.

11. Validation

The performance of the design algorithm has been extensively evaluated in the literature for various stationary passages and compressible flow configurations [14,15,31–33]. Here, a similar evaluation is performed in the case of incompressible flow in a rotating passage. To this end, the reduced static pressure is used as the target design parameter, which is expected to directly contribute to boundary layer thickening and flow separation due to adverse gradients [30]. The reduced pressure is calculated through the following expression:

$$P_{\text{reduction}} = P - \frac{1}{2}\rho\, r^2\omega^2. \tag{7}$$

To perform the validation, the geometry of the main pump is used as a target, and the initial geometry is constructed by applying arbitrary changes to the target geometry, as shown in Figure 10. The corresponding flow regime is laminar and incompressible, and the flow field is simulated by applying a uniform inlet velocity of 1.3 m/s and a relative pressure of zero at the outlet. Here, 25×50 cells are used for simulation. Despite the rotational nature of the flow passage as well as flow separation within the initial geometry, design convergence successfully occurs after 27 iterations, as shown in Figure 11.

To investigate the effect of design parameters on the performance of the algorithm, the static pressure is now considered for this purpose. Starting from the same initial conditions, the design procedure converges after only 56 iterations, as depicted in Figure 12. The effect of grid sizes on the design procedure is also investigated. For this purpose, the same computational domain with coarser (14×28) and finer (45×60) elements is considered. Figure 13 compares the convergent solution for the coarser domain against the reference case (25×50 elements). The results of the case with finer elements are not included in this figure, as the corresponding convergent solution overlaps that

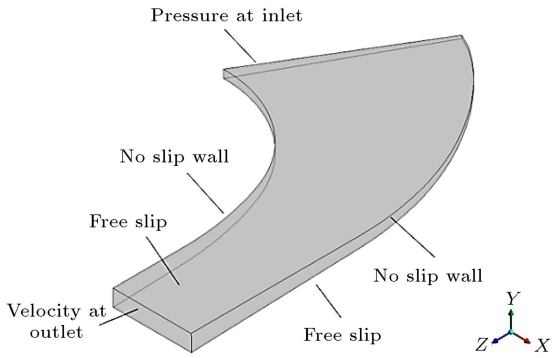

Figure 9. Created quasi-3D duct with boundary conditions.

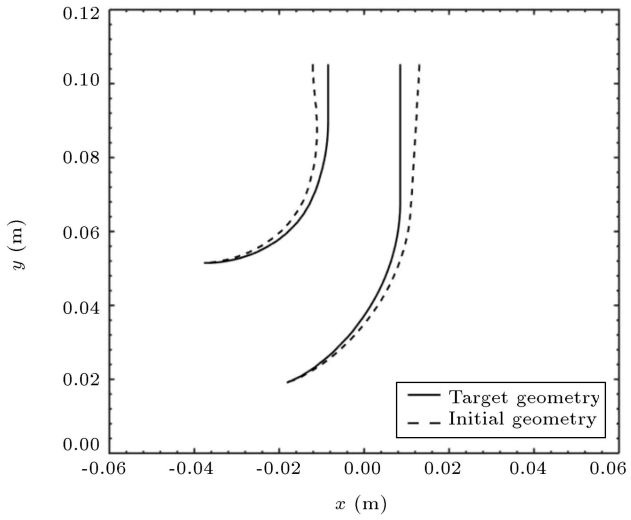

Figure 10. Initial guess and target geometry for validation.

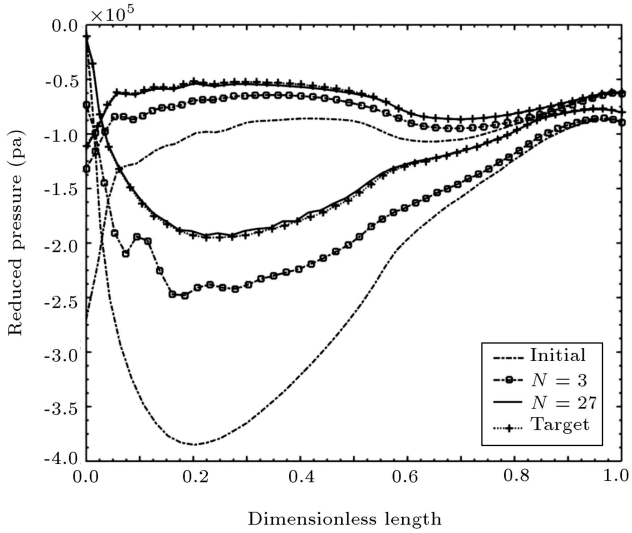

Figure 11. Converging process of reduced static pressure distribution from initial guess geometry to the target geometry.

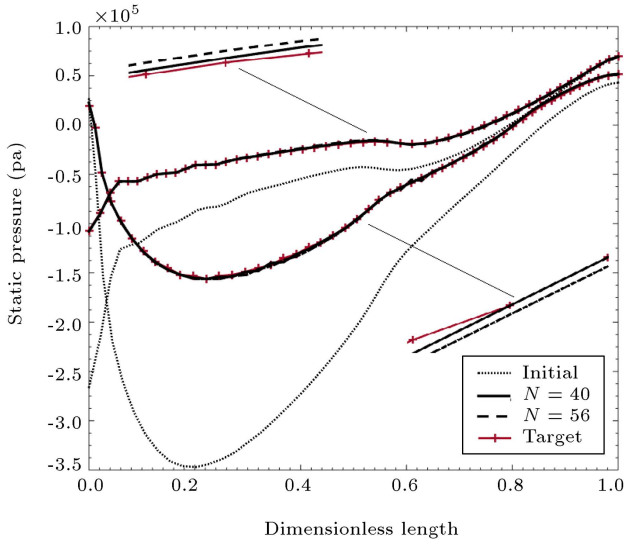

Figure 12. Converging process of static pressure distribution from the initial guess geometry to the target geometry.

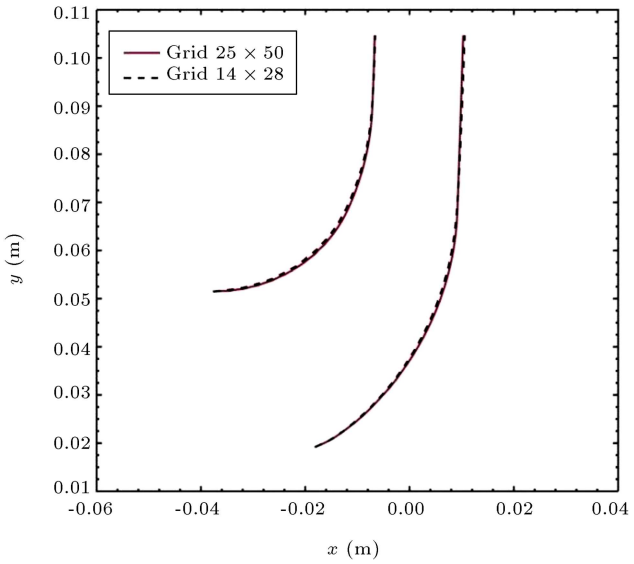

Figure 13. Grid study for design of the meridional plane in the rotating frame.

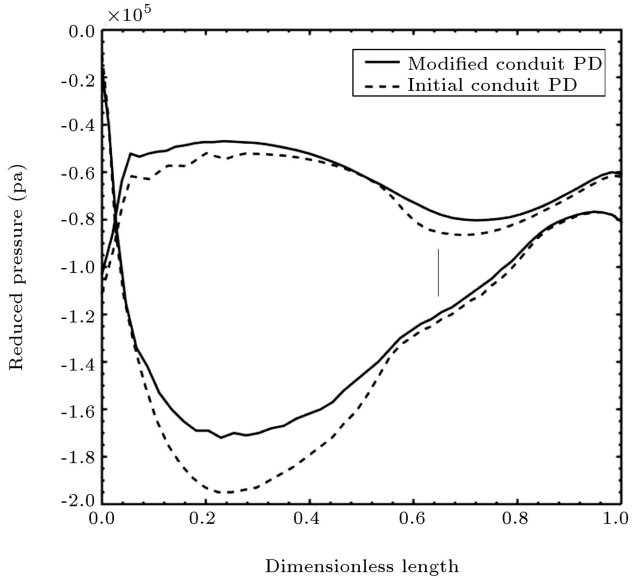

Figure 14. Current and modified reduced pressure distributions along the hub and shroud.

of the reference case. This suggests that the design algorithm becomes independent of element size beyond a certain threshold.

12. Geometry modification

The sharp curvature of impeller on the meridional plane is combined with the blade geometry results in wake and potential flow separation on the suction side of the shroud surface and is manifested as a pressure drop. In addition, high local velocities and unnecessary rapid flow accelerations (or decelerations) also contribute to the overall energy loss. On the other hand, the high angle of incidence at the flow inlet may also result in considerable energy loss, which requires design reconsideration. These design issues can be addressed on either the meridional or blade-to-blade planes of the impeller.

The validated design procedure is now employed to modify the pump geometry on the meridional plane. Figure 14 shows the current and target pressure distributions on the hub and shroud surfaces. The corresponding geometries, before and after the shape modification, are shown in Figure 15. The adjustment parameter C used in the current design procedure is 10^{-8}, and the full convergence of the design occurs after 34 iterations. In order to accurately examine

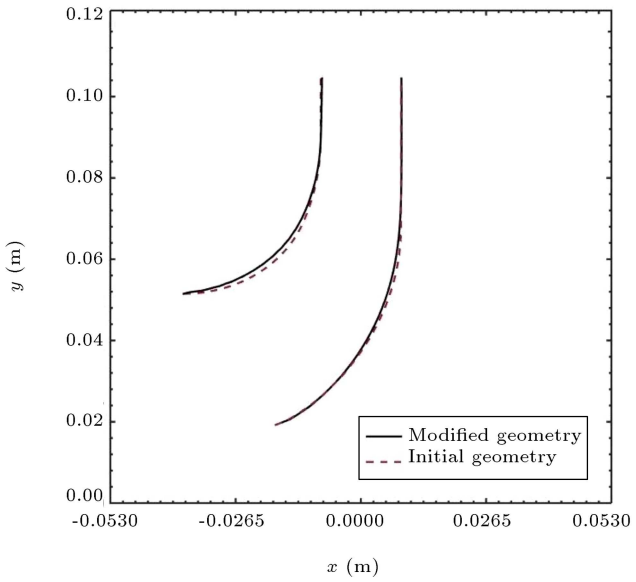

Figure 15. Current and modified geometry of the meridional plane.

Table 4. Values of dimensionless head and flow coefficients.

Geometry	ψ	φ
Original	0.577	0.102
Modified	0.605	0.107

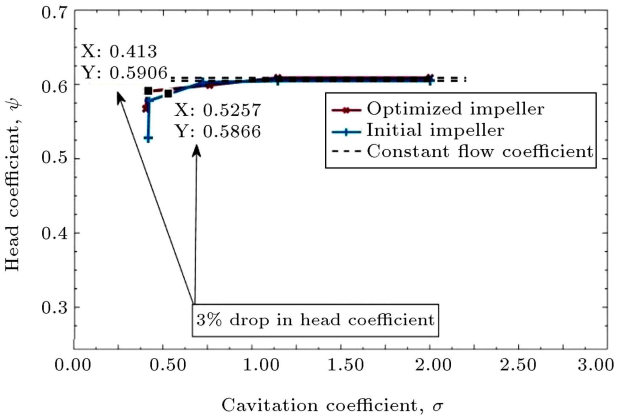

Figure 17. Cavitation operation curve for optimized and current impellers.

the resulting improvements, the full geometry of the modified impeller is constructed and evaluated using the 3D solver discussed earlier. The corresponding static pressure distribution in Figure 16 shows that the flow field on the suction side of the modified geometry has improved. Figure 16 shows that the velocity distribution at the outlet of the impeller has become more uniform for the modified geometry and the corresponding average value has increased. Table 4 summarizes the results of the final shape modification. It is important to note that the overall pump head has increased by over 5% for the modified geometry at BEP.

Figure 17 demonstrates the pump performance as a function of cavitation for the existing and modified pumps. In this graph, head coefficient is plotted against Thomas cavitation coefficient at BEP. The Hydraulic Institute standards have defined the cavitation onset as the point where a 3% drop occurs in pump head. Beyond this point, the local cavitation grows and considerable loss of pump performance is expected. After applying this criterion, Figure 17 shows that the cavitation onset is delayed for the modified geometry, suggesting that the modified pump can successfully operate under lower suction pressures.

13. Conclusion

In the current work, the ball-spine inverse design algorithm was developed as a quasi-3D method and was applied on the meridional plane of a centrifugal pump

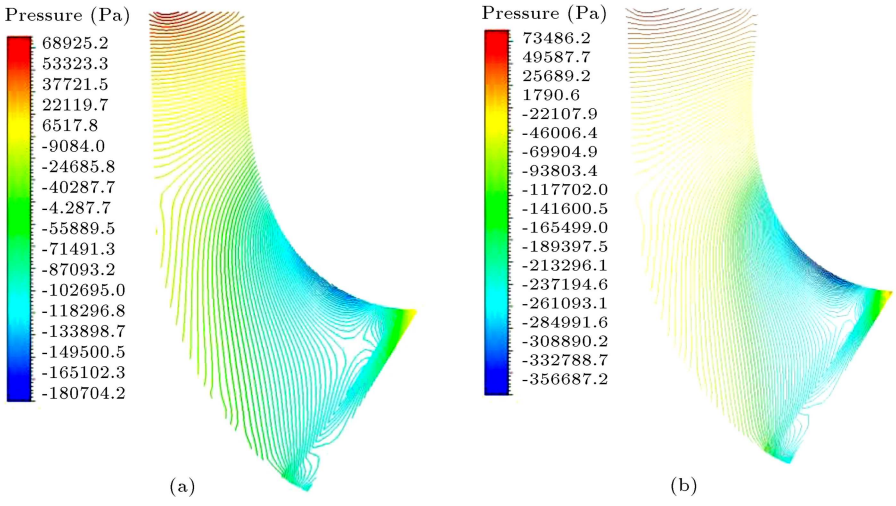

Figure 16. Static pressure contour on the created quasi-3D conduit: (a) Initial conduit and (b) modified conduit.

impeller operating in an incompressible, viscous flow regime. In this method, the viscous flow simulations were conducted within a thin region between two adjacent blades of an impeller, where the full 3D Navier-Stokes equations were solved instead of their inviscid, quasi-3D counterparts. The design algorithm was implemented using an external MATLAB code coupled with the ANSYS CFX as the flow solver. This approach further allows for the utilization of different spatial filters to smoothen the geometry at each step, which in turn allows the adjustment parameter of the design algorithm to be enhanced, hence improving the corresponding convergence rate. The results demonstrated that the reduced pressure distribution was a more physically meaningful design parameter than static pressure and it improved the convergence of the design algorithm. It was further found that the algorithm became independent of the grid size beyond a certain threshold. The developed design algorithm was finally applied to an existing pump in an effort to improve its performance by eliminating unnecessary, excessive pressure gradients on the meridional plane of the impeller. The simulation of the flow field within the modified impeller demonstrated an overall increase in pressure along the streamline, resulting in a delay in the cavitation onset on the suction side of the passage and a 5% improvement in the pump head.

Nomenclature

a	Acceleration of the ball (m/s^2)
A	Element area, diffuser cross-sectional area (m^2)
BSA	Ball-Spine Algorithm
C	Geometry correction coefficient (m^2 s^2 /kg)
m	Ball mass (kg)
ρ	Density of fluid (kg/m^3)
ρ_b	Density of ball (kg/m^3)
F	Force imposed on the ball (N)
P	Static pressure (Pa)
r	Radial coordinate, radius (m)
ω	Angular velocity (s^{-1})
Δ	Difference
Δt	Time step (s)
ΔP	Target and computed pressures difference (Pa)
φ	Flow coefficient
ψ	Head coefficient
BEP	Best efficiency point
PD	Pressure distribution
y^+	Non-dimensional wall distance
σ	Cavitation coefficient

References

1. Dang, T. and Isgro, V. "Euler-based inverse method for turbomachine blades. I-Two-dimensional cascades", *AIAA Journal*, **33**(12), pp. 2309–2315 (1995).
2. Dang, T., Damle, S., and Qiu, X. "Euler-based inverse method for turbomachine blades, part 2: three-dimensional flows", *AIAA Journal*, **38**(11), pp. 2007–2013 (2000).
3. Van Rooij, M., Dang, T., and Larosiliere, L. "Improving aerodynamic matching of axial compressor blading using a three-dimensional multistage inverse design method", *Journal of Turbomachinery*, **129**(1), pp. 108–118 (2007).
4. Qiu, X., Ji, M., and Dang, T. "Three-dimensional viscous inverse method for axial blade design", *Inverse Problems in Science and Engineering*, **17**(8), pp. 1019–1036 (2009).
5. Tiow, W. and Zangeneh, M. "Application of a three-dimensional viscous transonic inverse method to NASA rotor 67", *Proceedings of the Institution of Mechanical Engineers, Part A: Journal of Power and Energy*, **216**(3), pp. 243–255 (2002).
6. Yang, J. and Wu, H. "The solution existence and uniqueness of the inverse method based on transpiration boundary condition", *J. Propul. Technology*, **36**, pp. 579–586 (2015).
7. Demeulenaere, A. and Van den Braembussche, R. "Three-dimensional inverse method for turbomachinery blading design", *ASME 1996 International Gas Turbine and Aeroengine Congress and Exhibition*, pp. V001T01A007–V001T01A007 (1996).
8. Daneshkhah, K. and Ghaly, W. "Aerodynamic inverse design for viscous flow in turbomachinery blading", *Journal of Propulsion and Power*, **23**(4), pp. 814–820 (2007).
9. Roidl, B. and Ghaly, W. "Redesign of a low speed turbine stage using a new viscous inverse design method", *Journal of Turbomachinery*, **133**(1), p. 011009 (2011).
10. Mileshin, V.I., Orekhov, I.K., Shchipin, S.K., and Startsev, A.N. "3d inverse design of transonic fan rotors efficient for a wide range of rpm", *ASME Turbo Expo 2007: Power for Land, Sea, and Air*, pp. 341–352 (2007).
11. Van Rooij, M. and Medd, A. "Reformulation of a three-dimensional inverse design method for application in a high-fidelity CFD environment", *ASME Turbo Expo 2012: Turbine Technical Conference and Exposition*, pp. 2395–2403 (2012).

12. Zhu, Y.-L., Wang, Z.-M., Chen, H.-S., and Tan, C.-Q. "Full 3-D inverse design optimization method for turbomachinery blade", *Journal of Aerospace Power*, **27**(5), pp. 1045–1053 (2012).

13. Yang, J., Liu, Y., Wang, X., and Wu, H. "An improved steady inverse method for turbomachinery aerodynamic design", *Inverse Problems in Science and Engineering*, **25**(5), pp. 633–651 (2017).

14. Nili-Ahmadabadi, M. and Poursadegh, F. "Centrifugal compressor shape modification using a proposed inverse design method", *Journal of Mechanical Science and Technology*, **27**(3), pp. 713–720 (2013).

15. Poursadegh, F., Hajilouy-Benisi, A., and Nili-Ahmadabadi, M. "A novel quasi-3D design method for centrifugal compressor impeller on the blade-to-blade plane", *ASME 2011 Turbo Expo: Turbine Technical Conference and Exposition*, pp. 1155–1162 (2011).

16. Nili-Ahmadabadi, M. and Poursadegh, F. "Optimization of a seven-stage centrifugal compressor by using a quasi-3D inverse design method", *Journal of Mechanical Science and Technology*, **27**(11), pp. 3319–3330 (2013).

17. Madadi, A., Kermani, M., and Nili-Ahmadabadi, M. "Application of the ball-spine algorithm to design axial-flow compressor blade", *Scientia Iranica, Transactions B, Mechanical Engineering*, **21**(6), pp. 1981–1992 (2014).

18. Madadi, A., Kermani, M., and Nili-Ahmadabadi, M. "Aerodynamic design of S-shaped diffusers using ball-spine inverse design method", *Journal of Engineering for Gas Turbines and Power*, **136**(12), p. 122606 (2014).

19. Arbabi, A. and Ghaly, W. "Inverse design of turbine and compressor stages using a commercial CFD program", *ASME Turbo Expo 2013: Turbine Technical Conference and Exposition*, V06BT37A045-V06BT37A045 (2013).

20. Arbabi, A., Ghaly, W., and Medd, A. "Aerodynamic inverse blade design of axial compressors in three-dimensional flow using a commercial CFD program", *ASME Turbo Expo 2017: Turbomachinery Technical Conference and Exposition*, V02BT41A055-V02BT41A055 (2017).

21. Ramamurthy, R., Roidl, B., and Ghaly, W. "A viscous inverse design method for internal and external flow over airfoils using CFD techniques", *V ECCOMAS CFD* (2010).

22. Hajilouy-Benisi, A., Nili-Ahmadabadi, M., Durali, and Ghadak, M. "Duct design in subsonic and supersonic flow regimes with and without normal shock waves using flexible string algorithm", *Scientia Iranica*, **17**(3), pp. 179–193 (2010).

23. Chen, C., Zhu, B., Singh, P.M., and Choi, Y.D. "Design of a pump-turbine based on the 3D inverse design method", *KSFM J. Fluid Mach.*, **18**(1), pp. 20–8 (2018).

24. Lee, S. "Inverse design of horizontal axis wind turbine blades using a vortex line method", *Wind Energy*, **18**(2), pp. 253–66 (2015).

25. Albanesi, A., Fachinotti, V., Peralta, I., Storti, B., and Gebhardt, C. "Application of the inverse finite element method to design wind turbine blades", *Composite Structures*, **161**, pp. 160–72 (2017).

26. Luo, J., Tang, X., Duan, Y., and Liu, F. "An iterative inverse design method of turbomachinery blades by using proper orthogonal decomposition", In *ASME Turbo Expo 2015: Turbine Technical Conference and Exposition 2015 Jun 15*, V02BT39A026-V02BT39A026 (2015).

27. Muntean, S., Draghici, I., Gînga, G., Anton, L.E., and Baya, A. "Hydrodynamic design of a storage pump impeller using inverse method and experimental investigation of the global performances", *Wasser-Wirtschaft Extra*, **1**, pp. 28–32 (2015).

28. Moghadassian, B. and Sharma, A. "Inverse design of single-and multi-rotor horizontal axis wind turbine blades using computational fluid dynamics", *Journal of Solar Energy Engineering*, **140**(2), p. 021003 (2015).

29. GS, A. and Lal, S.A. "Inverse design of airfoil using vortex element method", *International Journal of Fluid Machinery and Systems*, **11**(2), pp. 163–70 (2018).

30. Greitzer, E.M., Tan, C.S., and Graf, M.B., *Internal Flow: Concepts and Applications*, Cambridge University Press (2007).

31. Nili-Ahmadabadi, M., Durali, M., and Hajilouy-Benisi, A. "A novel quasi 3-D design method for centrifugal compressor meridional plane", *ASME Turbo Expo 2010: Power for Land, Sea, and Air*, pp. 919–931 (2010).

32. Nili-Ahmadabadi, M., Poursadegh, F., and Shahhosseini, M.R. "Performance improvement of a centrifugal compressor using a developed 3D inverse design method", *ASME 2012 11th Biennial Conference on Engineering Systems Design and Analysis*, pp. 201–210 (2012).

33. Ahmadabadi, M.N., Ghadak, F., and Mohammadi, M. "Subsonic and transonic airfoil inverse design via ball-spine algorithm", *Computers & Fluids*, **84**, pp. 87–96 (2013).

Biographies

Hadi Fallah-Ardeshir is a PhD Candidate of Mechanical Faculty of Tabriz University. He received her Master's degree in Energy Conversion from School of Mechanical Engineering in Iran University of Science and Technology. Her research interests include turbomachinery.

Biyuk Ehghaghi is an Associate Professor and a Faculty Member at the Department of Mechanical

Engineering at Tabriz University of Technology. He received his Master and PhD degrees from Tabriz University respectively. His major research interests include the fields of turbomachinery, experimental aerodynamics, and manufacturing.

Mahdi Nili-Ahmadabadi is an Associate Professor and a Faculty Member of Mechanical Engineering Department at Isfahan University of Technology. He received his Master and PhD degrees from Sharif University of Technology in 2005 and 2010, respectively. His major research interests are inverse design, turbomachinery, experimental aerodynamics, and PIV measurement.